THESIS

ENGINEERING SYSTEM MODELING FOR SUSTAINABILITY ASSESSMENT

Submitted by

Jay Barlow

Department of Mechanical Engineering

In partial fulfillment of the requirements

For the Degree of Master of Science

Colorado State University

Fort Collins, Colorado

Fall 2016

Master's Committee:

Advisor: Jason C. Quinn

Bryan Willson
Kenneth F. Reardon

ABSTRACT

ENGINEERING SYSTEM MODELING FOR SUSTAINABILITY ASSESSMENT

The increase in global greenhouse gas emissions has driven interest in the development of renewable energy sources. The commercial development of emerging renewable technologies like algal biofuels requires the identification of an economically viable production pathway. This study examined the sustainability of generating renewable diesel via hydrothermal liquefaction (HTL) of algal biomass from an attached growth architecture. Pilot-scale growth studies and laboratory-scale HTL experiments validated an engineering system model, which facilitated analysis of economic feasibility and environmental impact of the system at full scale. Techno-economic analysis (TEA) results indicate an optimized minimum fuel selling price (MFSP) of \$11.90 gal^{-1}, and life-cycle assessment (LCA) found a global warming potential (GWP) of -44 g CO_2-e MJ^{-1} and net energy ratio of 0.33. Results from this work identified current gaps in sustainability assessment through TEA and LCA. Two needs were identified to improve sustainability assessment: the internalization of a carbon emission price into TEA and the consideration of the time-value of carbon emissions in LCA. With these effects considered, MFSP and GWP increase by 23% for the modeled biofuels system. Results from a harmonized model of an array of energy technologies indicate that prices for fossil-based energy increase 200% and GWP increases 25% when these factors are considered, whereas low-emitting technologies increase minimally in both metrics. Based on these findings, the development of improved sustainability assessment methodology is proposed.

ACKNOWLEDGEMENTS

I acknowledge Bryan Willson, Kenneth Reardon, Shantanu Jathar, Megan Kosovski, and the Powerhouse community for their contributions at Colorado State University. Many at Utah State University also supported this work: Ron Sims is acknowledged for his significant contributions and Hossein Jahromi, Jeffrey Moody, and Zak Fica for their technical assistance. I heartily thank Maureen Kesaano, Anna Doloman, and Iegor Pererva for their research and non-research contributions alike. I gratefully acknowledge the support of Jason Quinn, whose guidance and insights have been instrumental throughout.

TABLE OF CONTENTS

1 ATTACHED GROWTH ALGAL BIOREFINERY CASE STUDY

1.1 Introduction

A global increase in energy consumption combined with the environmental impact associated with fossil fuels has generated interest in producing renewable fuels. Algal biofuels are a promising renewable biofuel feedstock due to the high photosynthetic efficiency of algae and its potential for utilization of low-quality land and water. The commercial viability of algal-based biofuels is yet to be demonstrated and alternative production and conversion technologies are being explored. Hydrothermal liquefaction (HTL) represents a promising technology to convert algal biomass to biofuel. This process utilizes a wet algal feedstock and converts a high degree of the embodied feedstock energy into a biocrude. In contrast to fatty-acid methyl ester biodiesel, biocrude is chemically comparable to petroleum crude and can be refined into an array of drop-in fuels.

Algal biomass cultivation remains a significant technical barrier to commercial algal biofuel and bioproduct production. Cost of algal feedstock was the most significant determinant of biofuel selling price in economic evaluations of algal biofuel production by Davis et al. (2014a) and Jones et al. (2014) exploring fermentation of fractionated biomass and HTL conversion, respectively. The economics and environmental impacts of traditional suspended algal cultivation systems such as open raceway ponds (ORP) and photobioreactors (PBR) have been researched in detail (Beal et al., 2015; Borowitzka, 1999; Davis et al., 2016; Quinn and Davis, 2015; Richardson et al., 2012; Slade and Bauen, 2013). However, attached growth architectures, which include algal turf scrubbers (Adey et al., 2011) and a variety of mechanized biofilm reactors

(Gross et al., 2015a), including a rotating algal biofilm reactor (RABR) that generates a harvestable algal biofilm by rotating in wastewater (Christenson and Sims, 2012), have not been characterized in terms of economic viability and environmental impact.

Biofilm cultivation offers several advantages in comparison to suspended algal cultivation. Biofilm biomass is mechanically harvested from the growth substratum in a dewatered form, whereas suspended growth systems must undergo energy-intensive processes to produce a dewatered feedstock (Johnson and Wen, 2010; Ozkan et al., 2012). Flocculation, dissolved air flotation, and centrifugation, which account for a significant portion of algal feedstock cost and energy input, are therefore avoided in attached growth systems. In contrast to homogeneous suspended growth systems, biofilm cultures capture carbon directly from the atmosphere and exhibit increased resilience due to the diversity of the biofilm polyculture (Gross and Wen, 2014; Hamilton et al., 2014; Lohman et al., 2015). Disadvantages of attached growth systems include relatively low lipid content and high ash content (Johnson and Wen, 2010; Mulbry et al., 2008). The impact of these advantages and disadvantages at a systems level needs to be evaluated.

The objectives of this work are to understand the economic viability and environmental impact of an algal biofilm based biorefinery integrating representative experimental results for model validation. This work develops and leverages experimental data from a pilot-scale cultivation platform and lab-scale HTL reactor into an engineering system model. This system model represents the foundation that supported the evaluation of economic viability and environmental impact through techno-economic analysis (TEA) and life-cycle assessment (LCA). The model is constructed modularly to support the evaluation of alternative sub-processes and multiple scenarios. Specifically, the baseline scenario includes coupling an open-lagoon

wastewater treatment plant with a rotating algal biofilm reactor cultivation facility and HTL conversion plant. Subsequent scenarios consider integration of wastewater treatment and optimization of system performance parameters. Results include the performance of the system in terms of global warming potential, net energy ratio, and economics of generating renewable fuels. Discussion focuses on a sensitivity analysis, optimization of the process to minimize the minimum fuel selling price and environmental impact, and a direct comparison of results to literature.

1.2 Materials and Methods

This section first presents methods for the laboratory-scale HTL experiments, then describes the system model informed by experimental inputs followed by details on the LCA and TEA methods. Experimental work included the cultivation of algal biomass from a biofilm reactor, conversion of the biomass to biocrude by HTL, and downstream analysis of products to establish energy and mass balances. The system model grounded in these results includes the definition of the baseline scenario and description of alternative scenarios, which are intended to represent the performance of a near-term realizable system.

1.2.1 Hydrothermal liquefaction (HTL) of algal biomass

Mixed-culture algal biofilm biomass was generated from a RABR system constructed and operated as described by Christenson and Sims (2012). Biomass from three separate harvests was blended for homogeneity and had a solids content of 21% and ash content of 31%. Total solids content of the biomass was calculated as the fraction of stable oven-dry weight at 105 °C of wet weight. Ash content was calculated as the fraction of stable fired weight at 550 °C of dry weight. On a dry-weight basis, the biomass was 36% carbohydrate, 4% lipid, and 19% crude

protein. Carbohydrate content was measured by the sulfuric acid-UV colorimetric method (Albalasmeh et al., 2013). Lipid content was measured by a sulfo-phospho-vanillin method (Mishra et al., 2014). Biomass protein content was calculated by multiplying the total biomass nitrogen content by the factor 6.25 (Jones, 1931).

HTL reactions were conducted in triplicate in a 500-ml pressure reactor (Parr 4520, 4848 controller). Operating parameters were selected within the range of previously identified optimum values to be most representative of scale-up scenarios (Guo et al., 2015; Jones et al., 2014; Tian et al., 2014). Wet algal biomass was sealed in the reactor and the headspace was vented and then pressurized to 2 MPa with nitrogen. The reactor was heated at an average rate of 7.6 °C min^{-1} to 325 °C ± 6 °C, for a 60-min retention time upon reaching that temperature. Operating pressure ranged from 14.5-16.2 MPa with minor fluctuations in temperature. The reactor was vented after cooling to 40 °C with an internal water loop.

At the end of each reaction, the contents were extracted from the vessel in equal volume of dichloromethane (DCM). The mixture was agitated manually for 3 min and centrifuged at 3700 x g for 10 min. The aqueous layer was decanted and filtered (Whatman 541 filter). The nonpolar phase, containing DCM and biocrude, was also filtered (Whatman 541 filter). The solid phase was re-suspended in 100 ml DCM, agitated, and centrifuged and decanted twice more to ensure full recovery of biocrude. Solids retained by filtration were combined and dried at 105 °C. Trace water was separated from the nonpolar phase by a separatory funnel and combined with the aqueous fraction. The nonpolar extract was distilled at 40 °C to recover the DCM solvent, and then dried to a stable weight at 60 °C to remove trace water and solvent. The solvent extraction was used

to quantify the yield from the system and is not the modeled large-scale recovery method as detailed in section 2.2.4.

HTL products were analyzed to establish mass and energy balances. Elemental analysis of the algal feedstock, HTL solids, aqueous phase, and biocrude was conducted with a Flash 2000 Organic Elemental Analyzer (Thermo Scientific, Waltham, MA). Total nitrogen and total phosphorous content of the biomass and HTL aqueous phase was measured by Hach analysis kits (Hach Co., Loveland, CO). Higher heating value (HHV) of the algal feedstock and biocrude was measured by bomb calorimetry (IKA C-2000) and values were corrected for the formation of acids by titration with base solution. Biocrude conversion was calculated as mass of biocrude divided by feedstock ash-free dry weight (afdw), and gas mass was determined by difference.

1.2.2 System model

Economic feasibility and environmental impact of system scale-up were evaluated through the development of a modular system model. This engineering system model is constructed with sub-process models that were validated with experimental mass and energy balances as well as values from the literature where appropriate. The model includes RABR algae cultivation coupled with wastewater treatment, mechanical harvesting of algae, conversion of the wet algal biomass to biocrude by HTL, upgrading and refining to renewable diesel, and transportation and distribution of the products (Figure 1).

The system model considers six scenarios with varying inputs in order to examine a range of system performances (Table 1). All model scenarios consider the operational costs (op-x) and capital costs (cap-x) of each sub-process from cultivation through transportation and distribution.

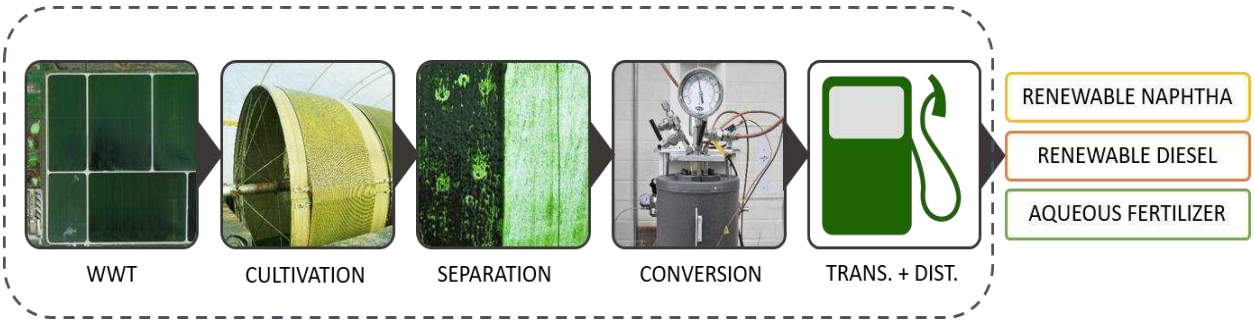

Figure 1: Process flow diagram of modeled system. Images depict Logan, Utah Lagoons wastewater treatment (WWT) facility, RABR cultivation, biomass separation by mechanical harvest, and lab-scale conversion by hydrothermal liquefaction to produce renewable diesel, naphtha, and aqueous fertilizer. Analyses were conducted within the indicated well-to-product system boundary (dashed line).

Table 1: Model scenarios and key inputs.

Scenario	Description	Productivity (g afdw m^{-2} d^{-1})	Biocrude yield (% afdw)	Cultivation area (acre)	WWT credit	RABR duty cycle
1	Base	12	21	460	None	1
2	Mid	20	30	460	None	1
3	WWT op-x	20	30	460	Op-x	1
4	WWT cap-x	20	30	460	Op-x, cap-x	1
5	Expanded	20	30	4600	Op-x, cap-x	1
6	Optimized	30	42	4600	Op-x, cap-x	0.5

To define a realistic base scenario, the conversion of the 460-acre Logan Lagoons wastewater treatment plant in Logan, Utah was modeled. The base scenario considers conservative algal productivity and the experimental HTL yield with a modeled annual output of 270,000 gallons of renewable diesel (RD). Mid-value productivity and HTL yield are considered in scenario 2. Scenarios 3 and 4 examine economic credits associated with displacement of wastewater treatment (WWT) op-x and cap-x, respectively. Scenario 5 adds an economy of scale achieved by expansion from a 460-acre to 4600-acre cultivation facility. A near-term realizable performance achieved by optimization of parameters is presented in scenario 6, with an annual output of 13.5 Mgal RD.

Cultivation process inputs were scaled from pilot-scale costs, energy inputs, and biomass yields. RABR capital costs were scaled with an economy of scale exponent of 0.6 to define a design-case RABR that is a seven-fold surface area expansion of the experimental architecture. The design-case RABR capital cost of \$40 m^{-2} accounts for a packing factor of 0.6 to accommodate balance of plant and maintenance access. An installation cost factor of 1.1 was applied to RABR capital costs. Labor for algae cultivation was estimated from Davis et al. (2016). Operational costs were based on scaled electricity consumption for RABR drive motors corresponding to 1 W m^{-2}. Case 6 considers a 50% reduction of this energy input by reduction of the drive motor duty cycle. Cost estimates for land, infrastructure, and site preparation were performed as described by Davis et al. (2016).

Base-case algal productivity was directly informed by experimental values and growth conditions in Logan, Utah and accounts for 3 months of zero productivity in the winter season and a summer productivity of 30 g afdw m^{-2} d^{-1} as reported by Christenson and Sims (2012)

resulting in an annual average of 12 g afdw m^{-2} d^{-1}. Productivity for model scenarios 2-5 is based upon separate RABR experiments that have achieved a six-month average of 20 g afdw m^{-2} d^{-1} and peak productivity of 45 g afdw m^{-2} d^{-1} for a combined annual average of 20 g afdw m^{-2} d^{-1}. Relocating the cultivation facility to a region with increased temperature and photosynthetically active radiation is expected to increase annual productivity to 30 g afdw m^{-2} d^{-1} (scenario 6) based on simulated results.

Algal biomass separation was modeled as direct mechanical harvest of the RABR surface by a stationary blade system. Separation capital cost was projected at 10% of RABR capital costs. A piping system for biomass collection was modeled with cost estimates as described by Davis et al. (2016). Energy associated with harvest was projected as a RABR drive power increase of 10% for the period of one RABR revolution, a weekly harvest frequency, and pumping requirements necessary to transport wet algal slurry from the center of the cultivation facility to a co-located HTL plant. Pumping energy requirements were calculated by modeling the algal slurry as a power-law fluid with an average consistency index from concentrated samples of 3 species (Wileman et al., 2012). Head requirements for slurry transport to the co-located HTL conversion facility include frictional losses for pipe length and apparatus as well as 10 m of head at the entrance of the HTL conversion plant. Installation cost factors of 1.2 and 1.4 were applied to piping and pumps, respectively.

Conversion process data were leveraged from Jones et al. (2014). Each conversion sub-process (HTL, catalytic hydrothermal gasification, hydrogen generation, and catalytic hydrotreating) was scaled according to experimental mass balances. Capital costs were scaled exponentially to varying production capacities with a whole-plant exponent of 0.7. The HTL gas

phase is assumed to be utilized as modeled by Jones et al. (2014), the aqueous phase is credited as a fertilizer co-product, and solids are assumed to be transported 50 km in a 22-ton truck. Fertilizer cost credit is based upon market values of comparable aqueous nitrogen and phosphorus products. The environmental impact of fuel transportation and distribution (T+D) is also included in the modeling effort.

The baseline biocrude yield of the system is based on the experimental data generated in this study. A yield of 30% is expected to be achieved with optimization of reaction parameters (scenarios 2-5). Separate HTL experiments performed on RABR biomass cultivated in oilfield produced water achieved a maximum yield of 38%, and further optimization of HTL parameters is expected to achieve a yield of 42% (scenario 6).

Wastewater is modeled to provide all necessary water and nutrients for algal cultivation based on previous RABR cultivation studies (Christenson and Sims, 2012) and municipal WWT data (Tchobanoglous et al., 2003). Algal nutrient removal during cultivation is considered to displace emissions and costs associated with treatment by conventional Bardenpho biological nutrient removal (BNR). Capital and operational costs for WWT displacement were obtained directly from Logan City, UT (2015) and average values from a survey of 16 BNR systems with capacities ranging from 0.1-150 MGD (US EPA, 2015). WWT displacement rate was based upon the stoichiometric nitrogen and phosphorous composition of the experimental biomass.

1.2.3 Techno-economic analysis

A discounted cash flow rate of return (DCFROR) analysis was conducted for the projected 30-year lifespan of the modeled system. For consistency with other system models reported in the literature, N^{th} plant assumptions were applied to all economic analyses, with key inputs

including a 10% internal rate of return, 35% income tax rate, and 8% interest on debt financing. Additionally, the capital costs of the RABR cultivation and separation facilities were projected to N^{th}-of-a-kind values based on experience curves as outlined by the National Energy Technology Laboratory (2013). Other operational costs including maintenance capital, insurance, and overhead were calculated as described by DOE design reports (Davis et al., 2012). Indirect capital costs, which include fees and other fixed expenses, were similarly considered. All economic analyses were scaled to year 2014 dollars based on the most recent data available from the Chemical Engineering Plant Cost Index for capital costs and the Bureau of Labor Statistics *Labor Indices Series ID CEU3232500008* for labor. The naphtha co-product price was fixed at \$3.25 gal^{-1}.

1.2.4 Life cycle assessment

LCA was conducted based on process data from the engineering system model. Net energy ratio (NER) and global warming potential (GWP) were determined for each process and are described further below. For consistency with other studies, LCAs were conducted within a well-to-product system boundary, i.e., processes including the production and distribution of fuel but excluding its combustion. All LCA results were normalized to the functional unit of 1 MJ of fuel product delivered to the commercial pump.

NER of the fuel production system was defined as the ratio of direct energy input to direct energy output. Energy inputs from each sub-process were summed and divided by direct energy outputs:

$$Net\ energy\ ratio\ (NER) = \frac{\sum direct\ energy\ inputs}{\sum direct\ energy\ outputs}$$

A value less than one represents an energetically favorable system. The modeled energy outputs included the renewable diesel product and the naphtha co-product.

The energy and mass balance from the experimental system model was used in combination with life-cycle inventory (LCI) data to quantify the environmental impact of the biorefinery. LCI data were extracted from the Argonne GREET model, the NREL LCI database, and the literature where appropriate (Jones et al., 2014). Greenhouse gas emissions were normalized to the metric of 100-yr GWP of carbon dioxide equivalent (CO_2-e). GWP values were calculated by combining emissions from carbon dioxide, methane, and dinitrogen monoxide with their respective equivalency factors of 1, 25, and 298, as defined by the Intergovernmental Panel on Climate Change (IPCC). Emissions were allocated to the combined fuel output of renewable diesel and naphtha and credited for atmospheric carbon uptake during cultivation, displacement of fertilizer production by the HTL aqueous phase co-product, and displacement of WWT energy as described by Sturm and Lamer (2011).

1.2.5 Sensitivity analyses

Sensitivity analyses were conducted on model inputs to identify impactful parameters for future research. Pertinent model inputs were varied by ±10% of base values and deviations from the corresponding model results were statistically analyzed with a least-squares model. To identify statistically significant model inputs, confidence intervals were constructed from a two-tailed t distribution at a significance level of 0.05.

1.3 Results and discussion

Experimental data generated from pilot-scale cultivation systems, results from HTL experiments, and pertinent data from literature were used to validate a modular engineering

system model. Mass and energy balances from this model served as the foundation to perform an economic and environmental impact assessment of an attached growth algal biorefinery. Six scenarios were modeled to evaluate alternative performance scenarios. The corresponding TEA and LCA results are presented for each scenario to highlight variations in system performance with results compared directly to the literature. Sensitivity analyses identify the most impactful system parameters for future research and development.

1.3.1 Hydrothermal liquefaction results

Biomass was harvested from a RABR representative of the modeled cultivation architecture. The biomass harvested had an ash content of 31% and lipid content of 4% on a dry-weight (dw) basis. These properties are consistent with other attached growth systems: Gross and Wen (2014) found ash and lipid contents of 29% and 8%, respectively, in biomass from a pilot-scale revolving biofilm reactor and Mulbry et al. (2008) reported ash content up to 49% in biomass from pilot-scale algal turf scrubbers. Direct mechanical harvest of the RABR yielded biomass slurry at 21% solids content, confirming that downstream dewatering prior to conversion through HTL is not required.

HTL experiments were conducted on RABR biomass to establish mass and energy balances for sub-process model validation. Biomass was converted to biocrude with a mean yield and standard deviation of 14.9±0.4% on a dry weight basis, corresponding to a mean yield of 21% afdw. Tian et al. (2015) achieved a comparable HTL biocrude yield of 18.4% afdw in a study of low-lipid (2% dw) and high-ash (41% dw) suspended biomass. Chen et al. (2014) demonstrated that HTL parameter optimization increased biocrude yield from 17.2% to 49.9% afdw in mixed-

culture algal biomass cultivated in wastewater. Such findings support the range of biocrude yields considered in the system model scenarios.

The mean dry weight yields and standard deviations of the aqueous, solid, and gas phases were 6.2±0.3%, 48.5±2.0%, and 30.4±2.5%, respectively. The HTL aqueous phase contains concentrated dissolved nitrogen and phosphorus that can displace traditional fertilizers as an aqueous co-product. The HTL aqueous phase had an average total nitrogen concentration of 5600 mg l^{-1} and total phosphorus concentration of 250 mg l^{-1} and these values were the basis for fertilizer displacement in all modeled scenarios.

Results from the experimental work were leveraged to validate the sub-process model used in the engineering system model. Conversion process data from Jones et al. (2014) were scaled according to the yields reported in this study, resulting in decreased relative fuel production capacity in the modeled biorefinery. The composition of the experimental biocrude was similar to that modeled by Jones et al. (2014), with average C, H, O, N, S, and ash contents of 73.6%, 8.6%, 10.9%, 5.3%, 0.4%, and 1.2%, respectively. The average biocrude HHV of 35.0 MJ kg^{-1} is in the mid-range of values widely reported in the literature (Biller and Ross, 2011). The sub-process model validated with these experimental data was integrated into the engineering system model for sustainability assessment work. A baseline mass balance around one unit of algal feedstock is depicted in Figure 2.

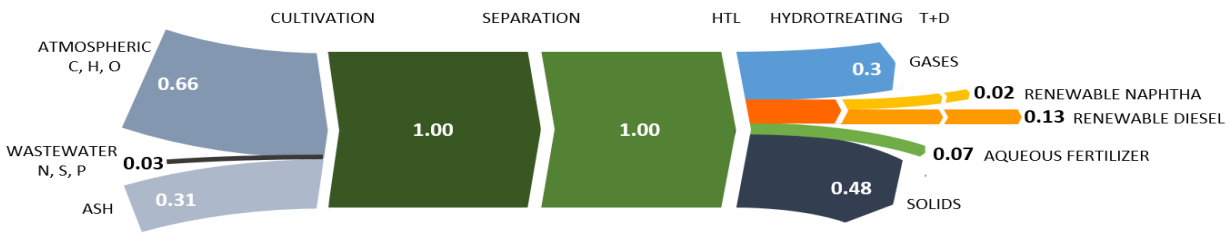

Figure 2: Baseline mass flow diagram for modeled process.

1.3.2 Techno-economic analysis

TEA was conducted to elucidate the economic viability of the biorefinery. A minimum fuel selling price (MFSP) was calculated to account for all cash flows over the lifetime of the plant. A separate economic analysis was conducted to determine a minimum algal feedstock selling price for the RABR cultivation process unique to this study and its effects on fuel selling price.

The MFSP in this study varies across the scenarios modeled (Figure 3). The baseline MFSP, modeled on conservative algal productivity and experimental biocrude yield, is \$104.31 gal^{-1}. Scenario 2 considers mid-range algal productivity and biocrude yield with a resulting MFSP of \$47.38 gal^{-1}. The displacement of WWT op-x and cap-x reduces MFSP to \$45.70 gal^{-1} (scenario 3) and \$40.60 gal^{-1} (scenario 4), respectively. Expanding the cultivation facility from 460 acres to 4600 acres achieves increased production capacity and capital economy of scale corresponding to a MFSP of \$28.63 gal^{-1} (scenario 5). A near-term realizable MFSP of \$11.90 gal^{-1} (scenario 6) is attained with increased algal productivity to 30 g afdw m^{-2} d^{-1} and biocrude yield to 42% as detailed in the methods. The economic viability of renewable fuels from the modeled system relies primarily on optimization of these parameters as discussed in the sensitivity results below.

Increased energy demand and capital costs arise from the high ash content of the biofilm biomass. Conversion plant infrastructure must be increased in scale to accommodate additional mass throughput, contributing to increased initial capital costs. The increased energy demand also translates into greater operating costs over the life of the plant. Such downstream effects alone account for a 49% increase in MFSP in the optimized modeled system compared to the results from Jones et al. (2014).

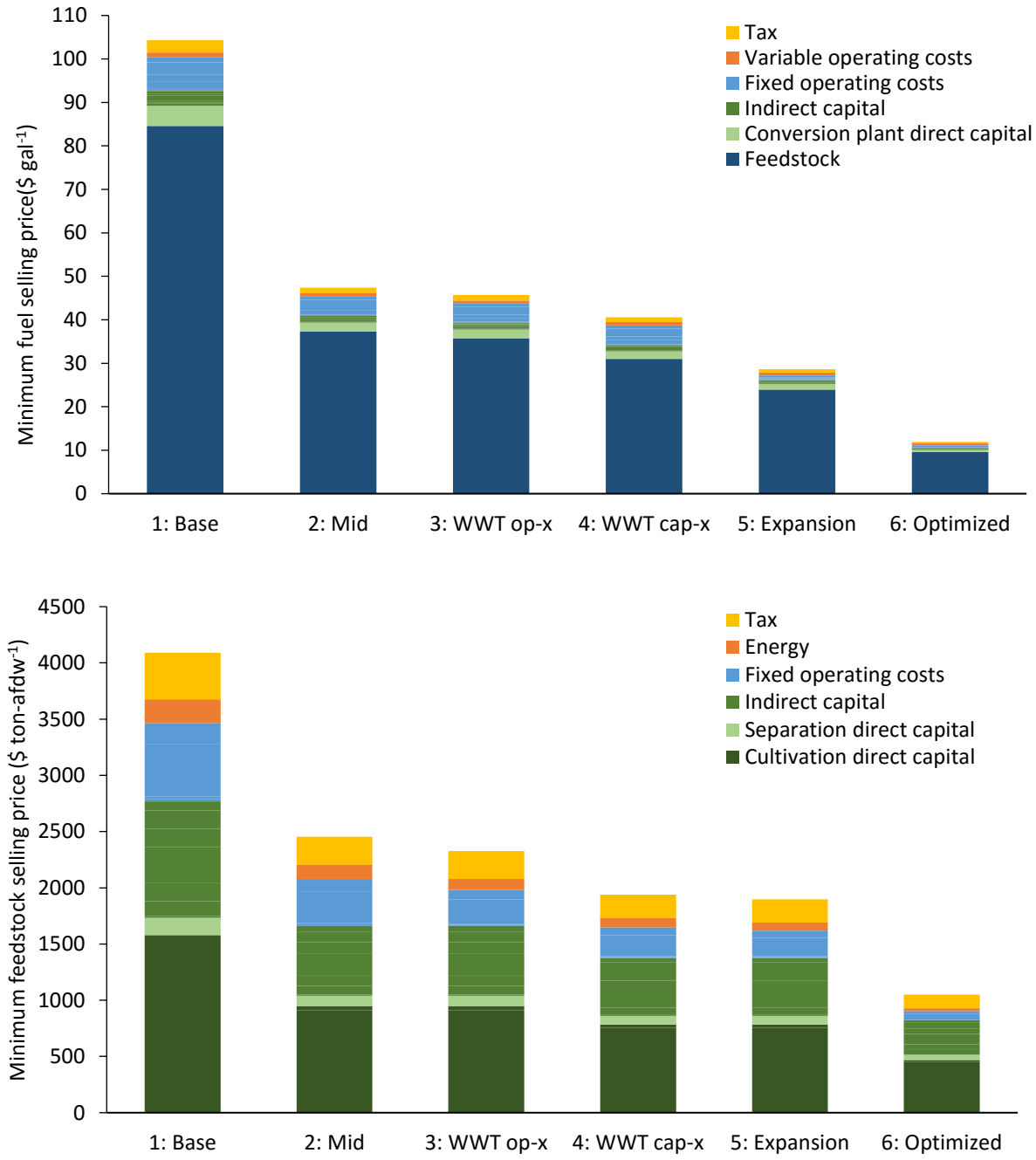

Figure 3: Categorized minimum fuel selling price (top) and minimum feedstock selling price (bottom). Model scenarios consider variations in modeled productivity, biocrude yield, and wastewater treatment (WWT) cost displacement.

The economic viability of numerous algal biofuels systems has previously been evaluated. MFSP results reported in the literature vary by feedstock type, conversion technology, and operating parameters. Davis et al. (2012) harmonized results for lipid-based fuels and determined a MFSP of \$19.60 gal^{-1} with conservative algal productivity. Laurens et al. (2015) attained a 33% reduction from this MFSP by modeling an alternative biochemical-based pathway for the conversion of algal lipids and carbohydrates. Summers et al. (2015) examined HTL conversion of oleaginous yeast and found a MFSP of \$4.78 gal^{-1}, a value similar to large-scale algal HTL conversion at a MFSP of \$4.77 gal^{-1} (Jones et al., 2014). These studies reflect MFSP reductions attained with economy of scale, low-cost feedstock, and increased yield associated with HTL conversion.

The near-term realizable MFSP in this study is supported by results from similar studies considering HTL pathways. Delrue et al. (2013) modeled an 800-acre cultivation facility with HTL conversion and found an average MFSP of \$10.18 gal^{-1}, which is comparable to the optimized scenario presented here. The similarity arises from comparable model inputs, which included algal productivity of 30 g m^{-2} d^{-1}, biocrude yield of 30-50%, and WWT integration. Davis et al. (2014b) modeled a large ensemble of geographic locations with ORP cultivation and HTL conversion. Though the average annual productivity in that study was 14.6 g afdw m^{-2} d^{-1}, the relatively high biocrude yield (59% afdw) and economy of scale associated with a 27 Mgal yr^{-1} HTL plant capacity yielded an average MFSP of \$9.80 gal^{-1}. When scaled to accommodate variations in algal productivity across the numerous sites considered, MFSP in that study increased to \$12 gal^{-1}, a value that aligns closely with scenario 6 in this study. The relatively high

MFSP for scenarios 1-4 in this study arise from conservative algal productivity and biocrude yield, limited production capacity, and high feedstock-related costs.

Biomass feedstock cost is the most influential component of MFSP, accounting for over 80% of the baseline MFSP (Figure 3). The optimized scenario (6) with a MFSP of \$11.90 gal^{-1} in this study is 150% greater than the \$4.77 gal^{-1} MFSP for an ORP-based system in a comparable system model (Jones et al., 2014). This can be primarily attributed to differences in feedstock costs, where a price of \$430 ton-$afdw^{-1}$ was assumed in the ORP study. Results from this study show, based on the optimized scenario (6), biomass price is \$1051 ton-$afdw^{-1}$. Secondary effects include a decreased biocrude yield and economy of scale in this study. Achieving the long-term DOE goal of \$3 per gallon gasoline equivalent (gge) with the modeled biofilm growth system would require a feedstock price of \$148 ton-$afdw^{-1}$, a seven-fold reduction from the optimized scenario.

To elucidate the economics of the attached growth system, the scope of the modular system model was narrowed to analyze the cultivation and separation sub-processes. Under experimental conditions, model results indicate a minimum feedstock selling price of \$4091 ton-$afdw^{-1}$ (Figure 3). Increasing productivity significantly reduces this price in the mid-range scenario (2) to \$2,455 ton-$afdw^{-1}$. Displacing WWT op-x only reduces biomass selling price by 5% (scenario 3), but significant savings are achieved by displacing wastewater treatment cap-x (scenario 4). Optimization of productivity and RABR drive energy reduces the selling price to \$1051 ton-$afdw^{-1}$ in scenario 6.

The minimum feedstock selling price is dominated by RABR capital costs. Capital costs account for 74% of the near-term realizable \$1051 ton-$afdw^{-1}$. A comparable economic model of

an open raceway pond (ORP) system by Davis et al. (2016) determined a minimum biomass selling price of \$491 ton-afdw^{-1}. This discrepancy can be largely attributed to the difference in capital cost between the two growth systems: RABR capital cost is five times greater than the ORP capital cost modeled by Davis et al. (2016), including the dewatering and CO_2 delivery costs in the ORP system that are avoided in the RABR system. The high capital cost of the RABR system is a reflection of the complexity and material requirements of mechanized biofilm reactors. A 90% reduction in capital cost would be required to attain the \$148 ton-afdw^{-1} feedstock price required for meeting the long-term DOE goal of \$3 gge^{-1} with an optimized RABR growth system. Design modification or extraction of a high-value biomass co-product would be required to attain such a reduction in biomass selling price.

Biofilm systems have demonstrated robust culture management that may lead to cost savings at scale. In contrast to single-strain open raceway ponds that undergo culture collapses, biofilm systems often utilize naturally occurring polycultures that exhibit increased stability. Gross and Wen (2014) demonstrated yearlong operation of a mechanized biofilm reactor at pilot scale, and Adey et al. (2011) achieved six months of continuous outdoor operation with a pilot-scale algal turf scrubber and a naturally selected polyculture. Furthermore, depth and turbidity do not limit most biofilm reactors due to direct exposure of the growth substratum to the atmosphere and these systems are therefore well adapted to integration with WWT for further cost savings (Kesaano and Sims, 2014). The robustness of the culture is directly coupled to the productivity, which is shown to be critically important to the economic viability.

1.3.3 Life-cycle assessment

The environmental impact of the biorefinery is presented in terms of NER to determine energy balance and GWP to describe impact from greenhouse gas emissions. Algal biofuels water consumption and wastewater integration are discussed based on literature review.

NER of each process was modeled to determine an energy balance of the biorefinery (Figure 4). NER was calculated as the ratio of direct energy input to direct energy output with favorable energy systems having a value less than 1. The baseline NER of 1.65 reflects the fact that more energy is invested in the fuel than is embodied in it. The most significant energy input is the RABR drive motor for biomass cultivation. Energy input for biomass separation by direct mechanical harvest and pumping of the biomass slurry is negligible in all scenarios and transportation and distribution of the fuel product accounts for less than 1% of total energy input. NER is comparable across scenarios 2-5, which consider variations in economic inputs that do not affect the energetics of the system. The optimized NER of 0.33 is achieved by high productivity, high yield, and reduction of the RABR drive motor duty cycle. The reduction of RABR drive duty cycle is a realizable method of reducing energy input while maintaining sufficient mechanical power for RABR rotation.

On a comparable well-to-product basis, the NER of conventional diesel is 0.19, and the NER of soybean biodiesel is 1.64 (Batan et al., 2010). These values span the range determined across the six model scenarios. In a study considering HTL and wastewater-coupled suspended cultivation, Delrue et al. (2013) found a NER of 0.5, which is comparable to the mid-range estimates in this study. Though baseline biofilm system performance is energy intensive,

optimization of RABR duty cycle, productivity, and yield can represent an energetically favorable system with a low NER.

GWP of the fuel product provides insight into environmental impact from greenhouse gas emissions (Figure 4). GWP values for the modeled scenarios closely reflect the energy inputs and outputs represented by NER but additionally include the upstream environmental burdens associated with energy and material production. The baseline scenario has a GWP of 79.7 g CO_2-e MJ^{-1}, with emissions from RABR drive energy and conversion outweighing the carbon credit attained by atmospheric uptake and WWT displacement.

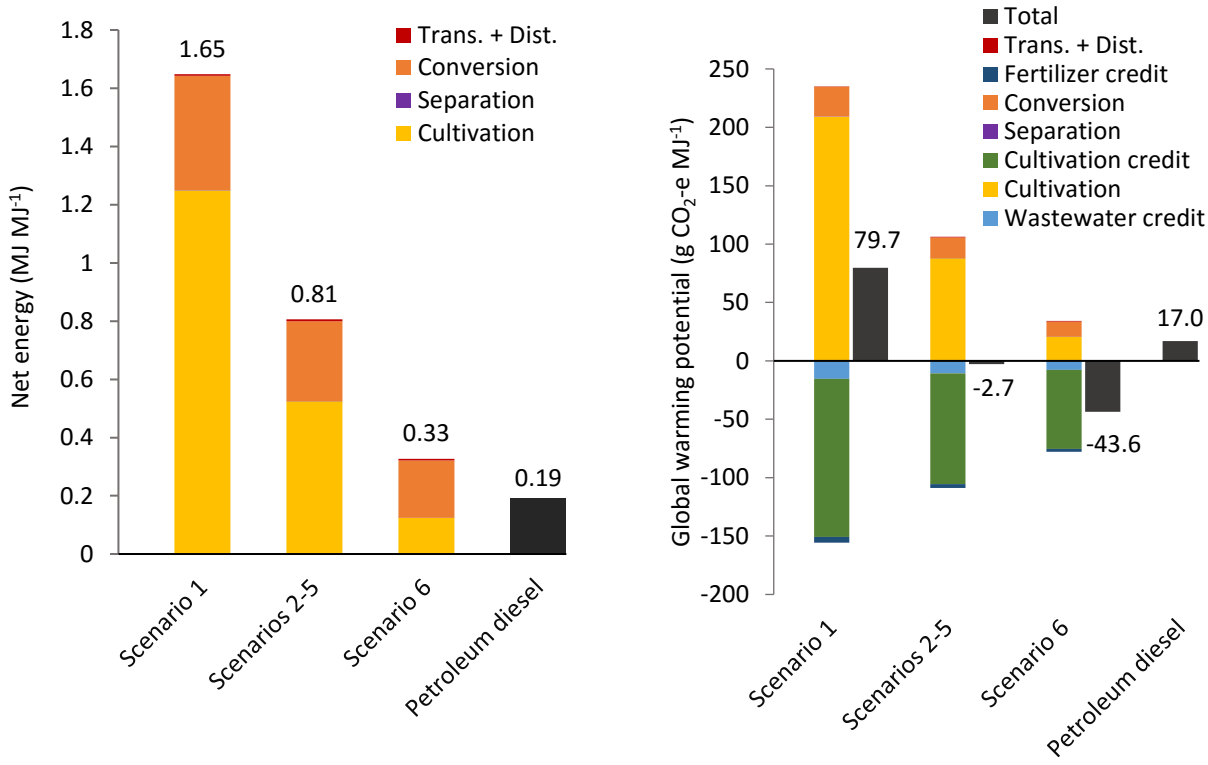

Figure 4: Net energy ratio (left) and global warming potential (right) of modeled scenarios. Results are normalized to functional unit of 1 MJ of fuel within a well-to-product system boundary. Energy and emissions contributions from the separation sub-process are minimal.

Scenarios 2-5, which consider variations in economic inputs that do not affect the environmental impact, consider mid-range productivity and biocrude yield and are nearly net-neutral at -2.7 g CO_2-e MJ^{-1}. Scenario 6 achieves a significant net-negative GWP from the combination of reduced RABR duty cycle, optimized algal productivity, and optimized biocrude yield at -43.6 g CO_2-e MJ^{-1}. In all cases, emissions from separation and T+D sub-processes are minimal.

Previously reported GWP values for algal biofuels systems range from -75 to 534 g CO_2-e MJ^{-1} (Quinn and Davis, 2015). Several researchers have examined algal HTL-specific conversion pathways with results varying according to system pathways and key input assumptions. Frank et al. (2013) found a GWP of -44 g CO_2-e MJ^{-1} for a system with a productivity of 25 g afdw m^{-2} d^{-1} and biocrude yield of 38% afdw. Using comparable inputs for productivity and yield, Delrue et al. (2013) additionally accounted for WWT integration and determined a GWP of -49.6 g CO_2-e MJ^{-1}. Both of these values align closely with scenario 6 in this study due to similar model inputs and process flows. Davis et al. (2014b) considered a lower productivity of 14.6 g afdw m^{-2} d^{-1} and accordingly found a higher GWP of -36 g CO_2-e MJ^{-1}. Model scenarios 2-5, which consider mid productivity and biocrude yield, are environmentally favorable in comparison to petroleum diesel, which has a GWP of 17 g CO_2-e MJ^{-1}. As expected, increasing the yields from the cultivation system and HTL conversion for scenario 6 results in an environmentally favorable system as well.

Life-cycle data are presented here on a well-to-product basis for consistency with other studies in the literature. Expansion to a well-to-wheels system boundary, which includes the emissions from fuel combustion, is assumed to contribute 74 g CO_2-e MJ^{-1} (Argonne National Laboratory, 2013). On a well-to-wheels basis, the GWP of modeled scenario 6 would be 30.4 g

CO_2-e MJ^{-1}, a 67% reduction compared to petroleum diesel. These findings indicate an environmentally favorable fuel product can be generated with optimized system parameters.

Water scarcity is a growing concern for energy systems. The most water-intensive process of algal biofuels systems is cultivation. Little is currently known about evaporative losses from mechanized biofilm cultivation architectures. Gross et al. (2015b) determined water losses from a revolving algal biofilm cultivation system to be 0.32 l g-biomass^{-1}. Assuming this rate is applicable to the RABR system, the cultivation losses would be 1420 gal-water gal-RD^{-1}. Water consumption for the conversion process was scaled from Jones et al. (2014) and found to be 5.1 gal-water gal-RD^{-1}, accounting for less than 1% of total water consumption in the modeled biorefinery. The aqueous phase produced by HTL may displace pristine irrigation water if used as aqueous fertilizer, but only accounts for 25 gal gal-RD^{-1}. Water consumption rates for algal biofuels reported in the literature range from 200 to 2000 gal-water gal-fuel^{-1} for ORP systems using transesterification to produce biodiesel (Tu et al., 2016). In a study of wastewater algal cultivation and HTL conversion, Delrue et al. (2013) modeled water losses of 260 gal-water gal-fuel^{-1}. For comparison, the water consumption for petroleum diesel is 5.6 gal-water gal-fuel^{-1} (Lampert et al., 2016).

The water-intensive nature of algal biofuels systems motivates the utilization of wastewater for algae cultivation. Nutrient demand of the modeled cultivation system could be met by municipal wastewater production. Assuming mid-range nutrient loading and average municipal production, the baseline nutrient demand could be satisfied by wastewater production of 4.5 MGD, corresponding to an approximate population of 45,000 people (Tchobanoglous et al., 2003). The optimized case, which considers high productivity and a 4600-acre facility, could

be satisfied by 110 MGD – the wastewater produced by a population of approximately 1.1 million people. These initial findings indicate that integrating algae cultivation with WWT can reduce pristine water consumption. Wastewater integration furthermore reduces biorefinery energy consumption, environmental impact, and product selling prices. Future resource evaluation needs to be completed to understand geographical limitations associated with co-location.

1.3.4 Sensitivity analysis

Sensitivity analyses of model inputs were conducted to determine their relative impact on resulting MFSP and NER (Figure 5). Sensitive inputs highlight areas for future research and optimization. Analysis indicates that algal productivity and biocrude yield are the most significant inputs for both MFSP and NER as expected. Optimization of algal productivity and biocrude yield will be most impactful in development of commercial-scale systems. Further optimization of algal productivity may be achieved by situating cultivation facilities in regions that support year-round operation. The base capital cost of the RABR is also a significant contributor to MFSP and reductions in this input may be attained by design modifications. Economic uncertainties surrounding co-product prices and the costs for land and civil work during facility preparation are not significant. A 10% variation of WWT displacement does not significantly affect either metric, though full-scale integration of WWT significantly reduces GWP and MFSP. Separation energy and several other inputs not listed here had no significant effect on either sustainability metric. Focusing future research on the most significant inputs will further reduce MFSP and NER values towards a commercially viable and environmentally sustainable biorefinery.

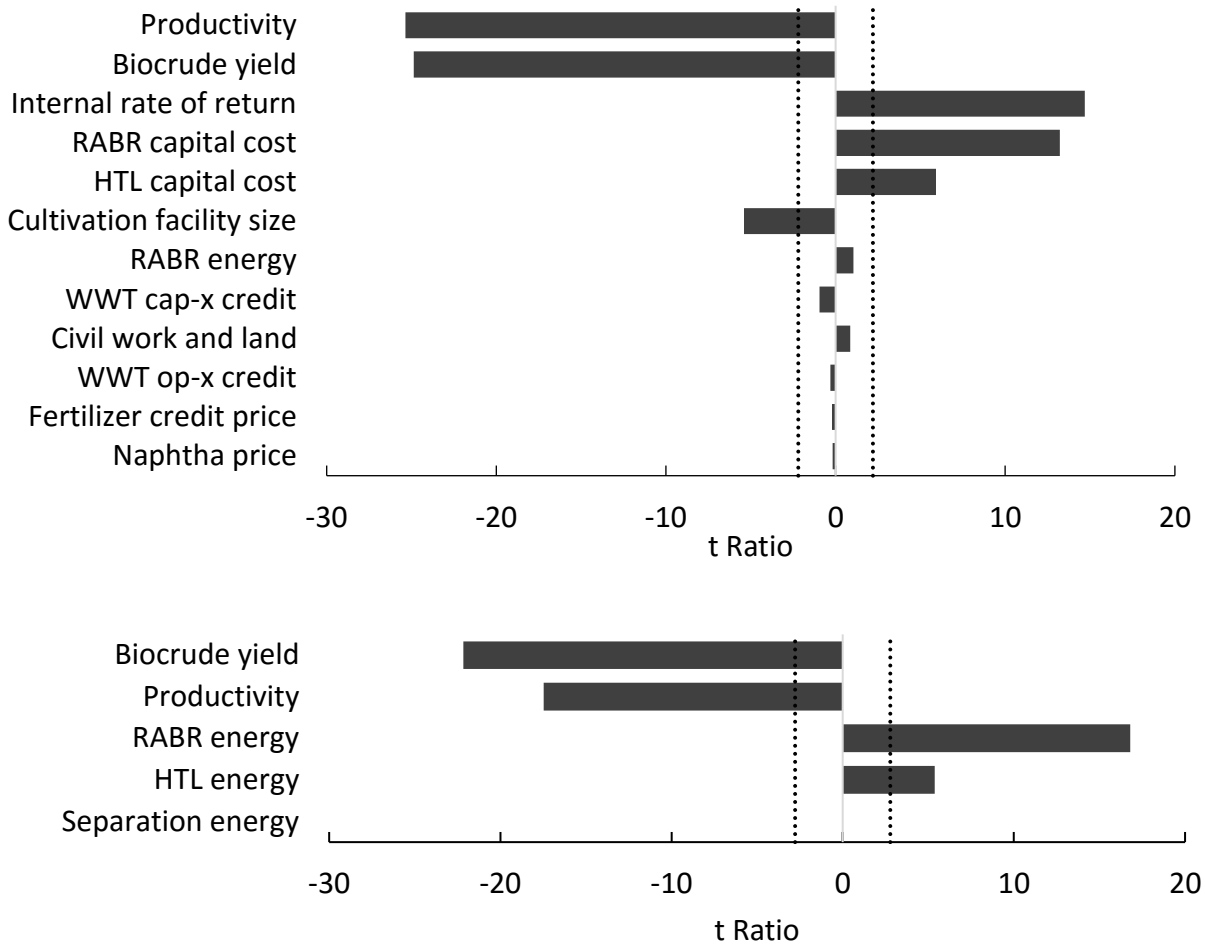

Figure 5: Sensitivity analysis of key inputs to minimum fuel selling price (top) and NER (bottom). Model parameters with t ratios exceeding 95% confidence intervals (vertical dashed lines) are considered statistically significant.

1.4 Conclusions

The systems-level impacts of integrating a biofilm cultivation system with WWT and HTL conversion were evaluated. A system model grounded in experimental results was developed to determine economic viability and environmental impact of an attached growth algal biorefinery. Techno-economic results indicate a range of MFSP values with a near-term realizable scenario of \$11.90 gal-RD^{-1}. Life-cycle assessment found a NER of 0.33 and GWP of -43.6 g CO_2-e MJ^{-1} under

optimized system parameters, reflective of an energetically and environmentally favorable system. Algal productivity and biocrude yield were determined to be the two most important factors affecting environmental impact and economic viability.

REFERENCES

Adey, W.H., Kangas, P.C., Mulbry, W., 2011. Algal turf scrubbing: cleaning surface waters with solar energy while producing a biofuel. BioScience 61, 434–441.

Albalasmeh, A.A., Berhe, A.A., Ghezzehei, T.A., 2013. A new method for rapid determination of carbohydrate and total carbon concentrations using UV spectrophotometry. Carbohydr. Polym. 97, 253–261.

Argonne National Laboratory, 2013. Greenhouse gases, regulated emissions, and energy use in transportation (GREET) model. Accessed 2015: https://greet.es.anl.gov/

Batan, L., Quinn, J., Willson, B., Bradley, T., 2010. Net energy and greenhouse gas emission evaluation of biodiesel derived from microalgae. Environ. Sci. Technol. 44, 7975–7980.

Beal, C.M., Gerber, L.N., Sills, D.L., Huntley, M.E., Machesky, S.C., Walsh, M.J., 2015. Algal biofuel production for fuels and feed in a 100-ha facility: A comprehensive techno-economic analysis and life cycle assessment. Algal Res. 10, 266-79.

Biller, P., Ross, A.B., 2011. Potential yields and properties of oil from the hydrothermal liquefaction of microalgae with different biochemical content. Bioresour. Technol. 102, 215–225.

Borowitzka, M.A., 1999. Commercial production of microalgae: ponds, tanks, tubes and fermenters. J. Biotechnol. 70, 313–321.

Chen, W.T., Zhang, Y., Zhang, J., Yu, G., Schideman, L.C., Zhang, P., Minarick, M., 2014. Hydrothermal liquefaction of mixed-culture algal biomass from wastewater treatment system into bio-crude oil. Bioresour. Technol. 152, 130–139.

Christenson, L.B., Sims, R.C., 2012. Rotating algal biofilm reactor and spool harvester for wastewater treatment with biofuels by-products. Biotechnol. Bioeng. 109, 1674–1684.

Davis, R., Fishman, D., Frank, E., Wigmosta, M., 2012. Renewable diesel from algal lipids: An integrated baseline for cost, emissions, and resource potential from a harmonization model. Natl. Renew. Energy Lab.: NREL/TP-5100-55431.

Davis, R., Kinchin, C., Markham, J., Tan, E., Laurens, L., Sexton, D., Knorr, D., Schoen, P., Lukas, J., 2014a. Process design and economics for the conversion of algal biomass to biofuels: algal biomass fractionation to lipid. Natl. Renew. Energy Lab.: NREL/TP-5100-62368.

Davis, R., Fishman, D.B., Frank, E.D., Johnson, M.C., Jones, S.B., Kinchin, C.M., Skaggs, R.L., Venteris, E.R., Wigmosta, M.S., 2014b. Integrated evaluation of cost, emissions, and resource potential for algal biofuels at the national scale. Environ. Sci. Technol. 48, 6035–6042.

Davis, R., Markham, J., Kinchin, C., Grundl, N., Tan, E., Humbird, D., 2016. Process design and economics for the production of algal biomass. Natl. Renew. Energy Lab.: NREL/TP-5100-64772.

Delrue, F., Li-Beisson, Y., Setier, P.A., Sahut, C., Roubaud, A., Froment, A.K., Peltier, G., 2013. Comparison of various microalgae liquid biofuel production pathways based on energetic, economic and environmental criteria. Bioresour. Technol. 136, 205–212.

Frank, E.D., Elgowainy, A., Han, J., Wang, Z., 2013. Life cycle comparison of hydrothermal liquefaction and lipid extraction pathways to renewable diesel from algae. Mitig. Adapt. Strateg. Glob. Change 18, 137–158.

Gross, M., Wen, Z., 2014. Yearlong evaluation of performance and durability of a pilot-scale Revolving Algal Biofilm (RAB) cultivation system. Bioresour. Technol. 171, 50–58.

Gross, M., Jarboe, D., Wen, Z., 2015a. Biofilm-based algal cultivation systems. Appl. Microbiol. Biotechnol. 99, 5781–5789.

Gross, M., Mascarenhas, V., Wen, Z., 2015b. Evaluating algal growth performance and water use efficiency of pilot-scale revolving algal biofilm (RAB) culture systems. Biotechnol. Bioeng. 112, 2040–2050.

Guo, Y., Yeh, T., Song, W., Xu, D., Wang, S., 2015. A review of bio-oil production from hydrothermal liquefaction of algae. Renew. Sustain. Energy Rev. 48, 776–790.

Hamilton, C., Rossmeissl, N., Ruddick, C., 2014. Exploring the utilization of complex algal communities to address algal pond crash and increase annual biomass production for algal biofuels. Accessed 2016: http://energy.gov/sites/prod/files/2014/04/f14/complex_algal_communities.pdf

Johnson, M.B., Wen, Z., 2010. Development of an attached microalgal growth system for biofuel production. Appl. Microbiol. Biotechnol. 85, 525–534.

Jones, D., 1931. Factors for converting percentages of nitrogen in foods and feeds into percentages of proteins. US Dep. Agric. 183, 1–21.

Jones, S.B., Zhu, Y., Anderson, D.M., Hallen, R.T., Elliott, D.C., Schmidt, A., Albrecht, K., Hart, T., Butcher, M., Drennan, C., 2014. Process design and economics for the conversion of algal biomass to hydrocarbons: whole algae hydrothermal liquefaction and upgrading. Pac. Northwest Natl. Lab.: PNNL-23227.

Kesaano, M., Sims, R.C., 2014. Algal biofilm based technology for wastewater treatment. Algal Res. 5, 231–240.

Lampert, D.J., Cai, H., Elgowainy, A., 2016. Wells to wheels: water consumption for transportation fuels in the United States. Energy Env. Sci. 9, 787–802.

Laurens, L.M.L., Nagle, N., Davis, R., Sweeney, N., Van Wychen, S., Lowell, A., Pienkos, P.T., 2015. Acid-catalyzed algal biomass pretreatment for integrated lipid and carbohydrate-based biofuels production. Green Chem. 17, 1145–1158.

Logan City, 2015. Logan City wastewater treatment master plan with appendix. Accessed 2016:http://www.loganutah.org/document_center/Environmenta/Logan%20City%20Wastewater%20Treatment%20Master%20Plan%20with%20Appendix_Oct15_2015.pdf

Lohman, E.J., Gardner, R.D., Pedersen, T., Peyton, B.M., Cooksey, K.E., Gerlach, R., 2015. Optimized inorganic carbon regime for enhanced growth and lipid accumulation in Chlorella vulgaris. Biotechnol. Biofuels 8, 82-95.

Mishra, S.K., Suh, W.I., Farooq, W., Moon, M., Shrivastav, A., Park, M.S., Yang, J.-W., 2014. Rapid quantification of microalgal lipids in aqueous medium by a simple colorimetric method. Bioresour. Technol. 155, 330–333.

Mulbry, W., Kondrad, S., Pizarro, C., Kebede-Westhead, E., 2008. Treatment of dairy manure effluent using freshwater algae: Algal productivity and recovery of manure nutrients using pilot-scale algal turf scrubbers. Bioresour. Technol. 99, 8137–8142.

National Energy Technology Laboratory, 2013. Technology Learning Curve. DOE/NETL-341/081213. Accessed 2016:

https://www.netl.doe.gov/File%20Library/research/energy%20analysis/publications/QGESS_FOAKtoNOAK_Final.pdf

Ozkan, A., Kinney, K., Katz, L., Berberoglu, H., 2012. Reduction of water and energy requirement of algae cultivation using an algae biofilm photobioreactor. Bioresour. Technol. 114, 542–548.

Quinn, J.C., Davis, R., 2015. The potentials and challenges of algae based biofuels: A review of the techno-economic, life cycle, and resource assessment modeling. Bioresour. Technol. 184, 444–452.

Richardson, J.W., Johnson, M.D., Outlaw, J.L., 2012. Economic comparison of open pond raceways to photo bio-reactors for profitable production of algae for transportation fuels in the Southwest. Algal Res. 1, 93–100.

Slade, R., Bauen, A., 2013. Micro-algae cultivation for biofuels: Cost, energy balance, environmental impacts and future prospects. Biomass Bioenergy 53, 29–38.

Sturm, B.S.M., Lamer, S.L., 2011. An energy evaluation of coupling nutrient removal from wastewater with algal biomass production. Appl. Energy 88, 3499–3506.

Summers, H.M., Ledbetter, R.N., McCurdy, A.T., Morgan, M.R., Seefeldt, L.C., Jena, U., Kent Hoekman, S., Quinn, J.C., 2015. Techno-economic feasibility and life cycle assessment of dairy effluent to renewable diesel via hydrothermal liquefaction. Bioresour. Technol. 196, 431–440.

Tchobanoglous, G., Burton, F., Stensel, D., 2003. Wastewater Engineering: Treatment and Reuse, fourth ed. McGraw-Hill, New York.

Tian, C., Li, B., Liu, Z., Zhang, Y., Lu, H., 2014. Hydrothermal liquefaction for algal biorefinery: A critical review. Renew. Sustain. Energy Rev. 38, 933–950.

Tian, C., Liu, Z., Zhang, Y., Li, B., Cao, W., Lu, H., Duan, N., Zhang, L., Zhang, T., 2015. Hydrothermal liquefaction of harvested high-ash low-lipid algal biomass from Dianchi Lake: Effects of operational parameters and relations of products. Bioresour. Technol. 184, 336–343.

Tu, Q., Lu, M., Thiansathit, W., Keener, T.C., 2016. Review of water consumption and water conservation technologies in the algal biofuel process. Water Environ. Res. 88, 21–28.

US EPA, 2015. A compilation of cost data associated with the impacts and control of nutrient pollution. EPA 820-F-15-096. Accessed 2016: https://nepis.epa.gov

Wileman, A., Ozkan, A., Berberoglu, H., 2012. Rheological properties of algae slurries for minimizing harvesting energy requirements in biofuel production. Bioresour. Technol. 104, 432–439.

2 TIME VALUE OF GREENHOUSE GAS EMISSIONS

2.1 Introduction

An engineering system modeling approach to sustainability assessment is grounded in mass and energy balances to describe direct economics, energetics, and greenhouse gas emissions. The system analysis can be expanded to examine additional impacts; water consumption, eutrophication potential, solid waste generation, and other aspects may be modeled. In the most comprehensive sense, sustainability assessment is defined by a consideration of impacts in the context of human and planetary welfare, in perpetuity. The diverse social, political, and economic aspects in this encompassing definition are inherently important to consider in sustainability assessment but often beyond the scope of engineering-based approaches. In this chapter I propose the incorporation of social costs and temporal weighting of greenhouse gas emissions in an effort to more holistically assess the sustainability of energy generation systems.

A holistic understanding of the economics and environmental burden of energy generation is necessary because impacts are typically realized over a long-term. A lock-in effect arises from the long-run nature of energy generation planning, with infrastructure investments and their associated impacts typically being committed for several decades or more (Unruh, 2000). Systems-level sustainability assessments, which may serve as the decision-making basis of energy generation investment, must therefore consider the time value of both economics and environmental impact.

Future carbon emissions are expected to cause greater relative damage than present emissions. This effect is reflected by the rising social cost of carbon (SCC), a measure of societal impact calculated by climate integrated assessment models. The SCC monetizes holistic detrimental effects of climate change including those on human health, agricultural productivity, and natural ecosystems (Interagency Working Group on Social Cost of Carbon, 2015). The physical basis for these increasing impacts arises from climate feedbacks such as changing albedo, increased releases of greenhouse gases, and potential reductions in carbon uptake capacity (Interagency Working Group on Social Cost of Carbon, 2011; Stern, 2007).

Current carbon accounting methods in sustainability assessment rely on a static metric of impact. Though the IPCC acknowledges the need for metrics to reflect the time value of emissions, it employs the static global warming potential index due to its transparency and comparability (IPCC, 2007). A global temperature potential has been proposed as an alternative to the GWP, but relies on the same underlying static principles. Temporal metrics have also been developed. Richards (1997) developed a temporal metric based on a marginal cost-benefit analysis. In a study of biofuels systems, Marshall (2009) expanded on this work to develop a physical discount rate for carbon accounting. These studies were based in the value of temporary carbon storage, however, and do not provide a common framework for evaluating the time value of impact on a physical basis alone. Furthermore, greenhouse gas emissions are not currently monetized in techno-economic analyses, resulting in market distortion and underestimation of the cost of energy.

The time value of economics and environmental impact must be integrated into sustainability assessment to provide a holistic assessment of committed impacts and viability. To

examine these effects, a harmonized TEA and LCA sustainability assessment model was constructed to analyze an array of energy generation technologies based on contemporary methodology. The model was adapted to evaluate the effects of internalization of SCC and temporal emissions impact factors derived from SCC models. Based on these findings, the discrepancy between current standard methods and time-value sustainability assessment is highlighted. Results from the work emphasize the need for improved methodology to evaluate the feasibility and impact of energy production technologies.

2.2 Methods

Harmonized TEA and LCA models were generated based on data from contemporary reviews. To facilitate the assessment of carbon pricing and temporal impact, emissions data were disaggregated into upstream burdens, occurring once at the outset of energy generation, and operational emissions, which occur for the remainder of the plant lifespan. Multiple scenarios were evaluated based on a range of SCC and corresponding derived impact factors. An array of technologies were analyzed based on data availability, technology maturity, and resource development capability at scale.

2.2.1 Techno-economic analysis

A harmonized discounted rate of return TEA model was utilized to calculate levelized cost of energy (LCOE) across the various technologies. In contrast to a conventional simplified LCOE analysis, harmonized financial inputs were implemented including an internal rate of return of 10%, debt interest rate of 8%, income tax rate of 10%, 60% debt financing of capital costs, and seven-year MACRS depreciation schedule on plant capital. Technology-specific inputs are listed in Table 2, with further details provided in subsequent sections.

Table 2: Key inputs to techno-economic analysis. NG=natural gas; PV=photovoltaic; CSP=concentrating solar power; CCS=carbon capture and sequestration.

Technology	Capital cost ($/kW)	Fixed O+M ($/kW-yr)	Variable O+M ($/kWh)	Capacity factor
Coal[1,2]	3246	31.60	0.0045	0.87
Coal-CCS[2]	5227	80.53	0.0095	0.87
NG[2]	1540	15.37	0.0033	0.85
NG-CCS[2]	2095	31.97	0.0068	0.85
PV[1,3]	2200	18.00	0.0000	0.20
CSP[1,3]	6300	65.00	0.0030	0.39
Nuclear[1]	5300	91.03	0.0006	0.90
Wind[1,3]	2200	60.86	0.0137	0.39

[1](US DOE, 2016) [2](US EIA, 2013) [3](IRENA, 2015)

2.2.2 Internalization of carbon price

SCC values were leveraged from updated estimates by the US Government (Interagency Working Group on Social Cost of Carbon, 2015). Briefly, estimates are derived from average values of three prominent climate integrated assessment models. Using emissions data as inputs, global temperature change and the resulting social damages are expressed as a distribution of prices per tonne emitted (Figure 6). Future damages are discounted across a 300-year horizon with an internal discount rate to generate three series of estimates: 2.5%, 3%, or 5%. A fourth estimate series is generated from the 95th percentile of the 3% model, representative of more severe future impact scenarios.

The TEA model was constructed to facilitate the evaluation of these alternative model estimates. SCC values from these model estimates were applied to time-resolved emissions data over a 30-year period over the years 2020-2050 to generate carbon emissions cash flows. These cash-flows were then integrated into baseline TEA models and the internalized LCOE was calculated for each SCC model scenario.

2.2.3 Life-cycle assessment

LCA was performed on each energy system to determine global warming potential of the energy product, based on data from contemporary reviews. Global warming potentials were normalized to the metric g CO_2-e kWh^{-1} by combining emissions from methane, dinitrogen monoxide, and carbon dioxide with their respective IPCC weighting factors. Emissions were disaggregated into upstream and operational burdens over the 30-year generation lifespan.

2.2.4 Temporal emissions impact factors

As a first approximation of the physical basis of increasing emissions impacts, emissions impact factors were derived from the SCC estimates, grounded in integrated assessment models (Figure 6). These relative impact factors, scaled to unity at year 2020, represent the relative burden of future emissions on a per-tonne basis. Impact factors were applied to time-resolved emissions data for each index year *i* over the project lifespan (n=30). Weighted emissions were then averaged over the energy generated, yielding a weighted GWP:

$$Global\ warming\ potential\ (GWP) = \sum_{i=1}^{n} \frac{Emissions_i \times Impact\ factor_i}{Generation_i}$$

Baseline GWP values were calculated with a static impact factor of one for each year.

2.2.5 Coal

Cost data were obtained from the US Energy Information Administration (US EIA, 2013). LCA data were obtained from median values in a contemporary review (Whitaker et al., 2012). The LCA model considers 1% of life-cycle emissions to occur as year-one upstream emissions, consistent with harmonized reviews. A 30-year plant lifespan is also analyzed by the majority of harmonized models. Carbon capture and sequestration (CCS) was considered by augmenting the

coal model with LCA data from Whitaker et al. (2012) and cost data from US EIA (2013) for an integrated gasification combined-cycle coal plant with post-combustion CCS.

2.2.6 Natural gas

Capital and operational cost data for natural gas combined-cycle plants were obtained from the US EIA (2013). LCA for natural gas generation facilities was based on a case study of a 555-MW combined-cycle plant with domestic gas supply as described by the National Energy Technology Laboratory (2012). Upstream and operational emissions were partitioned with 99.7% of life-cycle emissions attributed to operational fuel combustion. CCS was considered with data from the same sources.

2.2.7 Nuclear

Capital and operational cost data were obtained from the Department of Energy Transparent Cost Database (US DOE, 2016). LCI data were obtained from a harmonized review (Warner and Heath, 2012). LCA data were obtained for light water reactors due to data availability. The 40-yr operational lifespan considered in the harmonized review was truncated at 30 years for internal consistency.

2.2.8 Concentrating solar power (CSP)

To date, two predominant CSP architectures have been developed: parabolic trough and central receiver. Cost data were obtained from an average of these technologies (US DOE, 2016). LCA data were obtained from median values of a harmonized review of trough and central receiver technologies (Burkhardt et al., 2012).

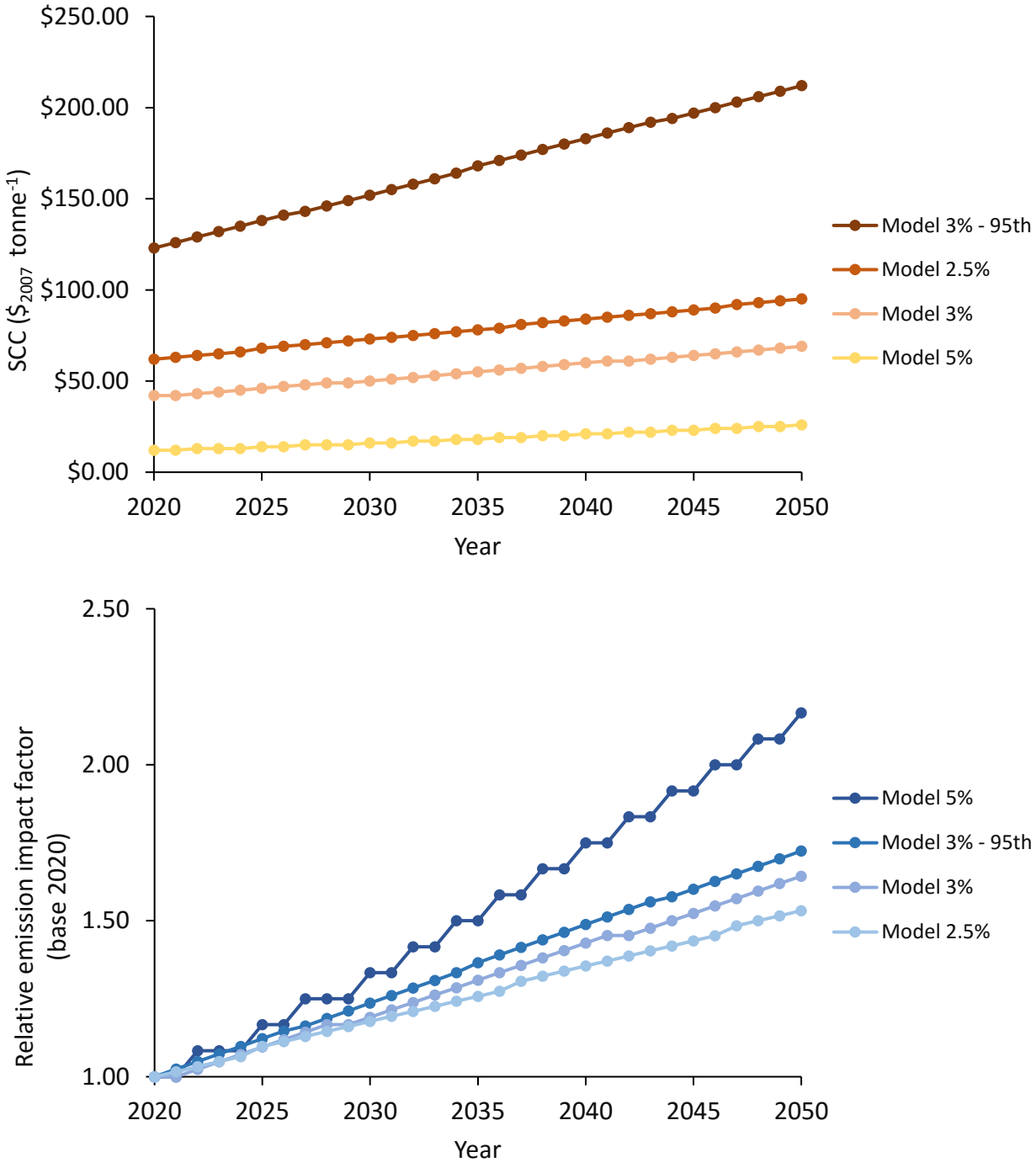

Figure 6: Social cost of carbon model estimates (top) and relative impact factors (bottom) derived from respective SCC model for the range years 2020-2050. Source: Interagency Working Group on Social Cost of Carbon, 2015.

2.2.9 Solar photovoltaic (PV)

Operational cost data were obtained from the Transparent Cost Database (US DOE, 2016). Capital cost data were obtained from the median of grid-scale capital cost estimates of global utility-scale projects installed in 2014 (IRENA, 2015). LCA data were obtained from a harmonized review of crystalline-silicon PV technologies (Hsu et al., 2012) and disaggregated into upstream and operational burdens attributing 0.1% of upstream manufacturing emissions to annual operations to account for maintenance and replacement of modules (Hou et al., 2016). Several of the studies projected facilities to outlast the analyzed 30-year lifespan.

2.2.10 Wind

Capital cost estimates for wind were obtained from the median of 2014 installed costs for large-scale onshore and offshore projects (IRENA, 2015). Operational costs and parameters were obtained from the Transparent Cost Database (US DOE, 2016). LCA data were obtained from a harmonized review (Dolan and Heath, 2012). Uncertainty surrounds the lifespan of large wind turbines, with most projected to last 20 years. However, several studies in the harmonized review considered 30-year lifespans (Hondo, 2005; Rydh et al., 2004; White and Kulcinski, 1998) and other researchers have identified a 30-year lifespan as more realistic (Jacobson, 2009). This study considers a 30-year lifespan by extending operational emissions.

2.3 Results and discussion

2.3.1 Techno-economic analysis

Baseline LCOE varies widely across the generation technologies analyzed (Figure 7). Fossil-fuel generation technologies, benefiting from market maturity, economy of scale, and low fuel price, represent the lowest LCOE. The analyzed renewable technologies have significantly higher

LCOE. Because fuel costs are minimal for these technologies, the high LCOE is dominated by capital and maintenance costs. These technologies are expected to experience significant future reductions in price with economy of scale and manufacturing experience, and efficiency gains in the case of PV (Alsema and de Wild-Scholten, 2006; IRENA, 2015, 2012).

LCOE increases in all cases upon internalization of SCC. Fossil generation technologies, with significant operational emissions, increase in LCOE significantly. The LCOE of coal increases 67% from baseline when the median SCC model is incorporated, and 200% when the maximum estimate is considered. Conversely, low-carbon technologies exhibit smaller increases in LCOE upon internalization of SCC, as expected. PV, which has significant upstream emissions but minimal operational emissions, increases only 1% in LCOE when the median SCC model is incorporated (4% when maximum estimate considered). Wind and nuclear generation, with minimal upstream and operational emissions, increase less than 1% upon internalization of the median SCC price estimates.

CCS can be applied to fossil-fuel generation technologies to reduce post-combustion emissions. The increased capital and operational costs associated with CCS give rise to a higher LCOE; coal-CCS has a baseline LCOE 69% greater than non-CCS coal generation. However, when median carbon prices are internalized, the two technologies have LCOE values within 10%. At higher SCC values, the avoided emissions charges offset the CCS costs: coal-CCS is 39% cheaper than non-CCS coal when the maximum carbon cost estimates are considered. A similar trend applies to natural gas generation.

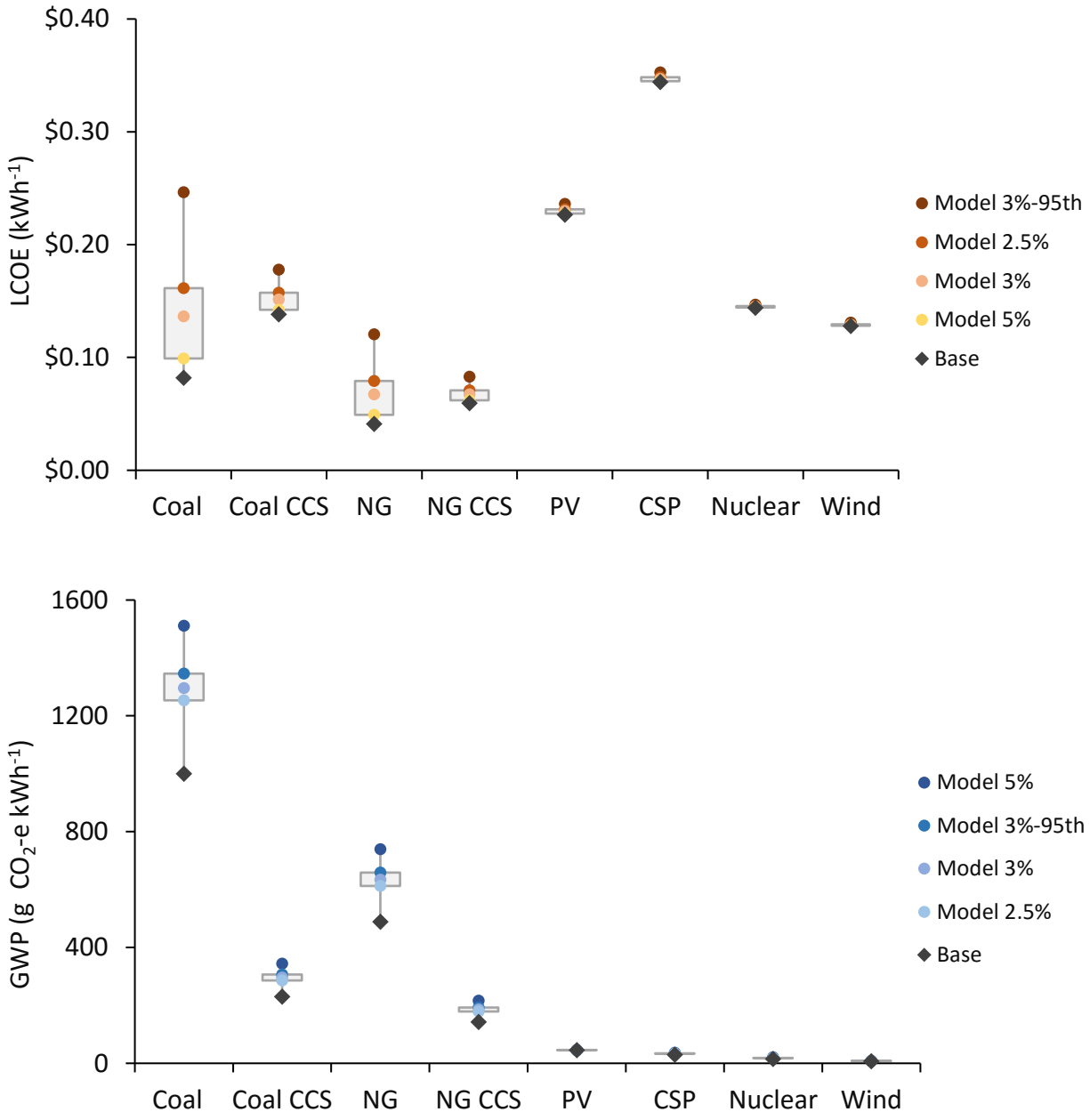

Figure 7: Levelized cost of energy (top) and global warming potential (bottom) across various generation technologies. Base values reflect harmonized average and model point estimates reflect values after integrating social cost of carbon or impact factor, respectively. Shaded boxes indicate median range of values. NG=natural gas; PV=photovoltaic; CSP=concentrating solar power; CCS=carbon capture and sequestration.

The internalization of carbon price presents an alternative view of LCOE and the subsequent decisions made for the deployment of energy generation technologies. Within the most probable range of LCOE values upon internalization of SCC prices, only PV and CSP are more expensive than coal generation. This finding suggests that the future energy mix could shift drastically to more economically favorable generation technologies if a carbon price was internalized in market LCOE. Furthermore, future SCC prices will increase, while renewable LCOE is expected to decrease, yielding a potential feedback towards low-emissions technologies dominating the future energy market. It should be noted that this analysis utilizes conservative SCC prices, with some researchers suggesting SCC may be six-fold greater than current median estimates (Moore and Diaz, 2015). Such findings emphasize the current market distortion in LCOE and the significance of internalizing emissions pricing.

2.3.2 Life-cycle assessment

The need exists to fully describe the environmental impact of energy generation, even when emissions costs are internalized. Baseline GWP values are static averages of emissions intensity per unit of energy produced and vary drastically by generation technology (Figure 7). A distinct dichotomy exists between the GWP of fossil and non-fossil energy generation technologies, with the former orders of magnitude greater than the latter. A 140-fold difference exists between the baseline GWP of coal, the highest emitting technology, and wind, the lowest emitting technology considered.

The application of temporal impact factors shifts the GWP from a static to a dynamic metric. This shift reflects the increased impact expected to arise from future emissions. When impact factors are incorporated into LCA, all technologies considered exhibit an increase in GWP.

Fossil generation technologies increase significantly upon weighting, whereas low-emission technologies increase minimally, as expected. Whereas coal exhibits a 30% increase in GWP with median estimates, wind exhibits an increase of only 3%. Solar PV, with a significant upstream emission but negligible operational emissions, increases less than 1%, even when maximum estimates for impact factors are incorporated. These findings highlight the current underestimation of the impact from fossil generation technologies.

The application of CCS to fossil energy generation lowers impact significantly. The baseline GWP of coal decreases 77% when CCS is applied. Natural gas follows a similar trend, with NG-CCS attaining a GWP 38% lower than coal-CCS generation. However, this GWP is still three-fold greater than that of PV, and 20-fold larger than wind, the lowest emitting technology considered. These discrepancies increase when impact factors are applied, reinforcing the dichotomy between fossil and non-fossil generation technologies in terms of global warming potential.

The weighted GWP analysis performed in this study was derived from integrated assessment models as an approximation of the physical mechanisms for future increases in emissions impact intensity. However, the need exists to develop an impact metric to directly reflect this physical basis in order to transparently elucidate the time value of emissions impacts. Alternative metrics have been proposed to correct the intentionally simplistic GWP defined by the IPCC. Global temperature potential (Shine et al., 2005), ton-year impact (Marshall and Kelly, 2010), or a new metric altogether may best define the true environmental impact committed by energy generation.

2.4 Conclusions

Current sustainability metrics fail to reflect the social cost of carbon and the time value of its emission. Internalization of the social cost of carbon increases fossil energy prices significantly, while low-emitting technologies remain relatively unchanged. Similar methodology was applied to evaluate global warming potential. Consideration of temporal impact factors to account for the increasing impact of future emissions increases GWP significantly for fossil energy sources and minimally for low-emitting sources. The resulting discrepancies between static and time-value sustainability assessment compel the development of improved sustainability assessment methodology.

REFERENCES

Alsema, E.A., de Wild-Scholten, M.J., 2006. Environmental impacts of crystalline silicon photovoltaic module production, in: Materials Research Society Symposium Proceedings. Warrendale, Pa.; Materials Research Society; 1999, 73.

Burkhardt, J.J., Heath, G., Cohen, E., 2012. Life Cycle Greenhouse Gas Emissions of Trough and Tower Concentrating Solar Power Electricity Generation: Systematic Review and Harmonization. J. Ind. Ecol. 16, S93–S109.

Dolan, S.L., Heath, G.A., 2012. Life Cycle Greenhouse Gas Emissions of Utility-Scale Wind Power: Systematic Review and Harmonization. J. Ind. Ecol. 16, S136–S154.

Hondo, H., 2005. Life cycle GHG emission analysis of power generation systems: Japanese case. Energy 30, 2042–2056.

Hou, G., Sun, H., Jiang, Z., Pan, Z., Wang, Y., Zhang, X., Zhao, Y., Yao, Q., 2016. Life cycle assessment of grid-connected photovoltaic power generation from crystalline silicon solar modules in China. Appl. Energy 164, 882–890.

Hsu, D.D., O'Donoughue, P., Fthenakis, V., Heath, G.A., Kim, H.C., Sawyer, P., Choi, J.-K., Turney, D.E., 2012. Life Cycle Greenhouse Gas Emissions of Crystalline Silicon Photovoltaic Electricity Generation: Systematic Review and Harmonization. J. Ind. Ecol. 16, S122–S135.

Interagency Working Group on Social Cost of Carbon, 2015. Technical Support Document:-Technical Update of the Social Cost of Carbon for Regulatory Impact Analysis-Under Executive Order 12866.

Interagency Working Group on Social Cost of Carbon, M., 2011. Estimating the social cost of carbon for use in US federal rulemakings: a summary and interpretation. National Bureau of Economic Research.

IPCC, 2007. Global Warming Potentials and Other Metrics for Comparing Different Emissions - AR4 WGI Chapter 2: Changes in Atmospheric Constituents and in Radiative Forcing Accessed 2016: https://www.ipcc.ch/publications_and_data/ar4/wg1/en/ch2s2-10.html

IRENA, 2015. Renewable Power Generation Costs in 2014.

IRENA, 2012. Renewable energy technologies cost analysis series: Concentrating Solar Power.

Jacobson, M.Z., 2009. Review of solutions to global warming, air pollution, and energy security. Energy Env. Sci 2, 148–173.

Marshall, E., Kelly, A., 2010. The Time Value of Carbon and Carbon Storage: Clarifying the terms and the policy implications of the debate. Available SSRN 1722345.

Marshall, L., 2009. Biofuels and the time value of carbon: Recommendations for GHG accounting protocols. WRI Work. Pap. 1–13.

Moore, F.C., Diaz, D.B., 2015. Temperature impacts on economic growth warrant stringent mitigation policy. Nat. Clim. Change 5, 127–131.

National Energy Technology Laboratory, 2012. Life Cycle Analysis: Natural Gas Combined Cycle (NGCC) Power Plant.

Richards, K.R., 1997. The time value of carbon in bottom-up studies. Crit. Rev. Environ. Sci. Technol. 27, 279–292.

Rydh, C.J., Jonsson, M., Lindahl, P., 2004. Replacement of old wind turbines assessed from energy, environmental and economic perspectives. Eur. Union Proj. Wind Energy Balt. Sea Reg. Final Rep.

Shine, K.P., Fuglestvedt, J.S., Hailemariam, K., Stuber, N., 2005. Alternatives to the global warming potential for comparing climate impacts of emissions of greenhouse gases. Clim. Change 68, 281–302.

Stern, N., 2007. The Economics of Climate Change: The Stern Review. Cambridge University Press.

Unruh, G.C., 2000. Understanding carbon lock-in. Energy Policy 28, 817–830.

US DOE, 2016. Transparent Cost Database. Accessed 2016: http://en.openei.org/apps/TCDB/

US EIA, 2013. Updated Capital Cost Estimates for Utility Scale Electricity Generating Plants.

Warner, E.S., Heath, G.A., 2012. Life Cycle Greenhouse Gas Emissions of Nuclear Electricity Generation: Systematic Review and Harmonization. J. Ind. Ecol. 16, S73–S92.

Whitaker, M., Heath, G.A., O'Donoughue, P., Vorum, M., 2012. Life Cycle Greenhouse Gas Emissions of Coal-Fired Electricity Generation: Systematic Review and Harmonization. J. Ind. Ecol. 16, S53–S72.

White, S., Kulcinski, G., 1998. Net energy payback and CO2 emissions from wind-generated electricity in the Midwest. Available: UWFDM-1092.